Fragile Histidine Triad (*FHIT*), a Novel Modifier Gene in Pulmonary Arterial Hypertension

Svenja Dannewitz Prosseda[1,2], Xuefei Tian[1,2], Kazuya Kuramoto[1,2], Mario Boehm[1,2], Deepti Sudheendra[1], Kazuya Miyagawa[2,3,4], Fan Zhang[2], David Solow-Cordero[5], Joshua C. Saldivar[6], Eric D. Austin[7], James E. Loyd[7], Lisa Wheeler[7], Adam Andruska[1], Michele Donato[8], Lingli Wang[1,2], Kay Huebner[9], Ross J. Metzger[2], Purvesh Khatri[8], Edda Spiekerkoetter[1-3]

Stanford University, Department of Medicine, Division Pulmonary and Critical Care[1], Wall Center for Pulmonary Vascular Disease[2], Cardiovascular Institute[3], Department of Pediatrics[4], High-Throughput Bioscience Center[5], Chemical and Systems Biology[6], Stanford, CA, Vanderbilt University Medical Center - Nashville, TN[7], Biomedical Informatics Research-ITI Institute[8], Ohio State University, Columbus, OH[9].

Online Data Supplement

METHODS

Pharmaceutical Reagents. In this study, Enzastaurin (Selleckchem, Houston, TX) and SUGEN5416 (Tocris, Bristol, UK) were used.

High Throughput siRNA Screen. High throughput siRNA screen of > 22,000 genes using an Id1-BRE luciferase reporter assay in a C2C12 mouse myoblastoma cell line treated with or without 250 pm BMP4 was conducted in the Stanford High-Throughput Bioscience Center, as previously described(E1). Briefly, C2C12 myoblastoma cells were stably transfected with BRE-Id1 linked to luciferase as a reporter cell line(E1) and screened on 72 x 384 well siRNA plates. The transfection conditions were optimized with BMP4 as stimulus, siBMPR2 and siTox as controls, DharmaFect3 as the transfection reagent and optimal concentrations for siRNAs (25nM) and cell numbers/well (1500). Target genes decreased Id1 expression to $\leq$ 60%, comparable to siBMPR2, while maintaining a general cell viability of $\geq$ 70% to exclude cell death response genes. Of the resulting 579 genes, unspecific genes, such as pseudogenes, RNA polymerase subunits, RNA splicing, transport factors and ribosome units were excluded in a secondary screening approach, yielded 96 genes, which were validated by target-specific siRNA pools. Hits were defined as a $\leq$ 60% reduction in Id1 expression, as well as a stricter cell viability criteria of $\geq$ 80% with a least 2 individual siRNAs. This yielded 74 gene candidates that were cross-validated using the novel meta-analysis approach.

Meta-Analysis

A novel integrated meta-analysis algorithm and a validation cohort was used to cross-validate the resulting list of 74 BMPR2 modifier gene candidates from the mouse myoblastoma HTS in seven publicly available human PAH transcriptomic datasets from the NCBI Gene Expression Omnibus (GEO) (Lung: GSE15197, GSE24988, GSE48149; PBMC: GSE19617, GSE22356, GSE33463, GSE703). All samples were uniformly curated using standardized vocabularies linked to the National Library of Medicine (NLM) United Medical Language System (UMLS), a parent vocabulary which includes Gene Ontology, SNOMED-CT, ICD-9, and ICD-10, as well as over a hundred other commonly used standardized vocabularies. The 7 PAH data sets comprised 291 samples from either PAH lungs (153 samples) or PBMCs (138 samples), which were used to develop a PAH dataset. We downloaded and manually curated each dataset, as previously described(E2-E5). Briefly, the data itself was normalized and converted to log2 using previously published methods(E6). We used two different meta-analysis approaches, called (i) combining fold changes and (ii) combining p-values as previously described(E7). Differentially expressed genes were selected that (i) had a specific false discovery rate threshold < 10%, and (ii) were expressed in the same direction (up- or downregulated) in at least 75% of the studies. To account for data dominance, caused by the unequal sample number, we removed one data set at a time for the meta-analysis.

The 74 targets from the mouse myoblastoma HTS were validated in human lung and PBMC PAH datasets to ensure that potential BMPR2 modifier genes were important in human PAH samples. A double screening approach was deemed necessary to account for healthy control subject variability, determining gene targets that are most relevant for human disease and most consistently regulated.

In addition to comparing the HTS siRNA results with the PAH gene expression datasets, we predicted an anti-PAH signature, which essentially is characterized by an opposite gene

expression to the PAH signature. The availability of gene expression profile datasets for drugs allows identification of FDA-approved drugs that may beneficial to treat PAH. We integrated a reference collection of gene-expression profiles from cultured human cells treated with bioactive small molecules. The database LINCS profiled a large number of drugs across many cell lines. LINCS is the largest database of gene expression profiles of cultured human cells treated with different drugs. At the time of analysis, there were 20,413 chemical perturbagens profiled on LINCS across 18 "gold" cell lines on the L1000 platform (www.lincscloud.org). With this technique we predicted which genes Enzastaurin and Dasatinib would target and whether the gene expression profile would be more similar to the PAH signature or anti-signature.

Animal Models. *Fhit* homozygous (-/-) mice were obtained from Kay F. Huebner (Ohio State University). *Bmpr2+/-* mice were a gift from Marlene Rabinovitch (Stanford University). Adult wildtype C57BL/6 mice, *Bmpr2+/-* or *Fhit-/-* mice at 8-10 weeks of age were housed in chronic hypoxia (10% O_2) for 3 weeks, followed by a recovery period of 4 weeks in normoxia (21% O_2), if indicated. *Bmpr2*+/- and *Fhit-/-* mice and littermates were treated with a daily dose of Enzastaurin (15 and 5 mg/kg body weight respectively) or vehicle for the duration of the study, administered through oral gavage.

Development of experimental PH was induced in adult Sprague Dawley rats (8 weeks old, 180-220g) through a single subcutaneous dose of the VEGF receptor tyrosine kinase inhibitor SUGEN5416 (20 mg/kg body weight), followed by exposure to chronic hypoxia (10% O_2) for 3 weeks and normoxia for 5 weeks (21% O_2), as previously described(E1). SuHx rats and littermates were treated with a daily dose of Enzastaurin (5 mg/kg body weight) or vehicle for 3 weeks, administered through oral gavage.

Right Ventricular (RV) Systolic Pressure was measured through right jugular vein catheterization and RV hypertrophy (RVH) was assessed by the weight ratio of the RV to left ventricle and septum (LV + S).

All animal experiments were approved by the Stanford University Institutional Animal Care and Use Committee.

Histology and ICC. Murine and rat lung tissue was fixed in paraformaldehyde (PFA) for 48 hours and preserved in EtOH. Paraffin embedded lung slides were stained with a Movat pentachrome stain (Histo-Tec, Hayward, CA), where vessel loss and muscularization of pulmonary vessels was visualized by light microscopy. Fluorescent immunocytochemistry on lung sections was performed on deparaffinized (Histoclear II, National Diagnostics) tissue sections with primary antibodies for von-Willebrand factor (vWF) and alpha smooth muscle actin (αSMA) following antigen-retrieval. Human PAH lung tissue was stained for anti-BMPR2 (Ab130206, Abcam) and anti-FHIT (kind gift of Kay F. Huebner, Ohio State University).

PFA-fixed paraffin-embedded heart tissue was stained with trichrome staining (Histo-Tec, Hayward, CA) to visualize fibrotic transformation.

Cell Culture. Human PAEC (Promocell) or human PASMC (Promocell) were grown as monolayers in gelatin-coated dishes in a commercial EC (Promocell) or SMC (Promocell) media, respectively. Cells were passaged at 1:3 ratios and used for experiments from passages 3-8. Transformed lymphocytes (i.e. lymphoblasts) were cultured in RPMI 1640 with 10-15% FBS.

Isolation of Cells from Human PAH Patients. PAEC of IPAH and FPAH patients at time of lung transplant were obtained from digested whole lung tissue, using CD31-AB pulldown beads (Dynabeads; Invitrogen), as previously described(E1). Peripheral Blood Mononuclear Cells (PBMCs) from were isolated from the peripheral blood of endstage PAH patients with negative *BMPR2* mutation status or healthy volunteers through Ficoll-Paque density gradient centrifugation, dextran sedimentation and RBC lysis, as previously described(E8). Lymphocytes from $BMPR2^{mut+}$ PAH patients and their unaffected relatives were isolated from the whole blood using gradient centrifugation and subsequently virally transformed, as previously described(E1). Experiments involving human tissue or derived primary cells were approved by the Stanford University Institutional Review Board and the Administrative Panel on Human Subject Research.

RNA Interference. FHIT expression was modulated by RNAi in PA endothelial cells (PAEC). A pool of 4 siRNAs for BMPR2, FHIT, LCK or a non-targeting control pool (Dharmacon) were transfected into PAECs using the RNAi Max kit (Invitrogen) for 48 hours. mRNA knockdown efficiency was determined by qPCR.

qPCR Assay to Detect mRNA and miR Expression. For mRNA, total RNA was extracted from whole lung tissue using the RNAeasy Plus Kit (Qiagen) and reverse transcribed into cDNA using random primers with the Taqman cDNA reverse transcription Kit (Applied Biosciences) according to the manufacturer's instructions. For miR, total miR was isolated from whole lung tissue using the Taqman miRNA ABC purification Kit (Applied Biosciences) and was reverse transcribed using specific primers and the Taqman microRNA reverse transcription kit (Applied

Biosciences). mRNA and miR expression levels were quantified using Taqman primer/probe sets for the target and normalized to a housekeeping control (mRNA: GAPDH; miR: RNU48).

Western Blotting. Western blotting was performed as previously described (E1). Antibodies for BMPR2 (Ab130206, monoclonal, Abcam), FHIT (NBPI-89061, polyclonal, Novus Biologicals; Ab180806, polyclonal, Abcam), PKC (Ab76016, monoclonal, Abcam), P-PKC (Ab32376, [Y124], monoclonal, Abcam), LCK (NBPI-19840, polyclonal, Novus Biologicals), p38 (Ab31828, monoclonal, Abcam), Id1 (sc133104, monoclonal, Santa Cruz Biotechnology), Smad1 (#9743, Cell Signaling), P-Smad1/5/9 (#13820P, Cell Signaling) and β-Actin (Sc47778, monoclonal, Santa Cruz) were used.

Apoptosis, DNA Damage, MTT Proliferation and Matrigel Tube Formation Assays. Assays were conducted according to the manufacturer's instructions and as previously described(E1,E9).

Deep Tissue Imaging. Deep tissue imaging of agarose-inflated lungs was conducted on a Leica M205FA fluorescent stereomicroscope using a Hamamatsu Orca Flash 4.0LT camera as previously described(E10,E11). Arterial muscularization in agarose-inflated lungs was assessed in arteries accompanying the left lobe secondary lateral airway branch L4 (L:L4)(E10) and was designated as branching generation 1 before the point of its bifurcation. Further descendant artery branch generations, generated by bifurcation or domain branching alike, were designated as branch generations 2-12. An increase in generation numbers was apparent for generations 6-10 in *Fhit-/-* mice, whereas wildtype mice did not exceed generation 7 of muscularized vessels.

Statistical Analysis. Data were analyzed using GraphPad Prism version 7.00, GraphPad software (La Jolla, CA). Statistical tests were performed as appropriate and included the following: Student's t-test, One-Way ANOVA and Two-way ANOVA, followed by the appropriate post-hoc test, as indicated. Bars show mean ± SEM. Differences were considered to be statistically significant as follows: $p<0.05$ (*/#), $p<0.01$ (**/##), $p<0.001$ (***/###), $p<0.0001$ (****/####).

DISCUSSION OF SUPPLEMENTAL FIGURES E1, E2

Sex specific differences in male vs. female *Fhit-/-* mice in susceptibility to loss of FHIT in hypoxia.

The occurrence of PAH is greatly increased in female patients, despite the more severe disease phenotype in males, where it rapidly leads to right heart failure(E12), as replicated in some animal models(E13,E14). Despite extensive research, the role of estrogen in PAH remains enigmatic, with both protective and deleterious effects reported(E15). We propose here that baseline FHIT expression is protective and may be a variable to explain sex differences in PAH, as steady-state FHIT levels are higher in men than in women(E16).

As reported for *ApoE-/-* and *VIP-/-* mice(E13,E14), two PAH models with sex-specific differences, we observed a more severe phenotype in male *Fhit-/-* mice. Whereas in *Fhit-/-* females, cardiovascular disease presented spontaneously, the RV adapted to hypoxia and the increases in RVSP were less dramatic in response to acute hypoxia, suggesting the presence of low-grade PAH at baseline, when FHIT is not present. In contrast, male *Fhit-/-* mice lacked a severe pulmo-vascular phenotype in normoxia; however, the acute response to hypoxia induced a mal-adaptive response in RVH and thus RV pressure, which was poorly reversible upon return to normoxia, suggesting that the RV in male *Fhit-/-* mice may be less apt to maintain homeostasis, paving the way for earlier right heart failure than in females. In support, it has been reported that FHIT levels are typically higher in men than in women(E16), suggesting that a loss of FHIT in males may elicit a more severe increase in hemodynamic parameters in the course of the hypoxia adaptation response. As only muscularization was increased in male *Fhit-/-* mice with no changes in RVSP pressures and RVH, this may indicate that the loss of pulmonary vessels was

not severe enough to elicit an increased pressure in the RV and thus no compensatory response by the RV was required.

The severe acute hyperresponsive increase in RVSP of male *Fhit-/-* mice to hypoxia, resembles the clinical phenotype, where acute RV failure is more commonly observed in male PH patients. In contrast, female *Fhit-/-* mice lacked a hyperresponsive RVSP increase in hypoxia; however, the increased RVSP, RVH and vessel loss at baseline in female, but not male *Fhit-/-* mice, argues for the presence of low-grade PAH in steady-state. However, the differences in RVSP pressure in normoxia between the sexes may also be accounted for by the more severe loss of pulmonary vasculature in female *Fhit-/-*.

While BMPR2 is undeniably a downstream target of FHIT, the presence of further BMPR2-independent, PAH-related downstream targets of FHIT is conceivable. In support, whereas we observed a uniform downregulation of BMPR2 in male and female FPAH patients in transformed lymphocytes, FHIT expression was unilaterally decreased in female FPAH patients only, which would link reduced FHIT to the more frequent occurrence of PAH in women(E18) Yet, the data in FHIT levels in health and disease are conflicting, given that others have described increased levels of FHIT in women(E17). Further research is required to correlate FHIT levels in female and male mice and men and the correlation with severity of disease. Interestingly, FHIT loss was observed more frequently in malignant compared to benign mammary carcinoma(E19) in menopausal women, supporting the importance of FHIT in the female sex.

REFERENCES

E1. Spiekerkoetter E, Tian X, Cai J, Hopper RK, Sudheendra D, Li CG, El-Bizri N, Sawada H, Haghighat R, Chan R, Haghighat L, de Jesus Perez V, Wang L, Reddy S, Zhao M, Bernstein D, Solow-Cordero DE, Beachy PA, Wandless TJ, Ten Dijke P, Rabinovitch M. FK506 activates BMPR2, rescues endothelial dysfunction, and reverses pulmonary hypertension. *J Clin Invest* 2013; 123: 3600-3613.

E2. Chen R, Khatri P, Mazur PK, Polin M, Zheng Y, Vaka D, Hoang CD, Shrager J, Xu Y, Vicent S, Butte AJ, Sweet-Cordero EA. A meta-analysis of lung cancer gene expression identifies PTK7 as a survival gene in lung adenocarcinoma. *Cancer Res* 2014; 74: 2892-2902.

E3. Khatri P, Roedder S, Kimura N, De Vusser K, Morgan AA, Gong Y, Fischbein MP, Robbins RC, Naesens M, Butte AJ, Sarwal MM. A common rejection module (CRM) for acute rejection across multiple organs identifies novel therapeutics for organ transplantation. *J Exp Med* 2013; 210: 2205-2221.

E4. Li MD, Burns TC, Morgan AA, Khatri P. Integrated multi-cohort transcriptional meta-analysis of neurodegenerative diseases. *Acta Neuropathol Commun* 2014; 2: 93.

E5. Lee KC, Ouwehand I, Giannini AL, Thomas NS, Dibb NJ, Bijlmakers MJ. Lck is a key target of imatinib and dasatinib in T-cell activation. *Leukemia* 2010; 24: 896-900.

E6. Drăghici S, Sellamuthu S, Khatri P. Babel's tower revisited: a universal resource for cross-referencing across annotation databases. *Bioinformatics* 2006; 22: 2934-2939.

E7. Benjamini Y, Drai D, Elmer G, Kafkafi N, Golani I. Controlling the false discovery rate in behavior genetics research. *Behav Brain Res* 2001; 125: 279-284.

E8. Spiekerkoetter E, Sung YK, Sudheendra D, Scott V, Del Rosario P, Bill M, Haddad F, Long-Boyle J, Hedlin H, Zamanian RT. Randomised placebo-controlled safety and tolerability trial of FK506 (tacrolimus) for pulmonary arterial hypertension. *Eur Respir J* 2017; 50.

E9. Chen PI, Cao A, Miyagawa K, Tojais NF, Hennigs JK, Li CG, Sweeney NM, Inglis AS, Wang L, Li D, Ye M, Feldman BJ, Rabinovitch M. Amphetamines promote mitochondrial dysfunction and DNA damage in pulmonary hypertension. *JCI Insight* 2017; 2: e90427.

E10. Metzger RJ, Klein OD, Martin GR, Krasnow MA. The branching programme of mouse lung development. *Nature* 2008; 453: 745-750.

E11. Sheikh AQ, Misra A, Rosas IO, Adams RH, Greif DM. Smooth muscle cell progenitors are primed to muscularize in pulmonary hypertension. *Sci Transl Med* 2015; 7: 308ra159.

E12. Austin ED, Lahm T, West J, Tofovic SP, Johansen AK, Maclean MR, Alzoubi A, Oka M. Gender, sex hormones and pulmonary hypertension. *Pulm Circ* 2013; 3: 294-314.

E13. Hansmann G, Wagner RA, Schellong S, Perez VA, Urashima T, Wang L, Sheikh AY, Suen RS, Stewart DJ, Rabinovitch M. Pulmonary arterial hypertension is linked to insulin resistance and reversed by peroxisome proliferator-activated receptor-gamma activation. *Circulation* 2007; 115: 1275-1284.

E14. Said SI, Hamidi SA, Dickman KG, Szema AM, Lyubsky S, Lin RZ, Jiang YP, Chen JJ, Waschek JA, Kort S. Moderate pulmonary arterial hypertension in male mice lacking the vasoactive intestinal peptide gene. *Circulation* 2007; 115: 1260-1268.

E15. Dempsie Y, MacLean MR. The influence of gender on the development of pulmonary arterial hypertension. *Exp Physiol* 2013; 98: 1257-1261.

E16. Czarnecka KH, Migdalska-Sęk M, Domańska D, Pastuszak-Lewandoska D, Dutkowska A, Kordiak J, Nawrot E, Kiszałkiewicz J, Antczak A, Brzeziańska-Lasota E. FHIT promoter methylation status, low protein and high mRNA levels in patients with non-small cell lung cancer. *Int J Oncol* 2016; 49: 1175-1184.

E17. Zheng H, Tsuneyama K, Takahashi H, Miwa S, Nomoto K, Saito H, Masuda S, Takano Y. Expression of PTEN and FHIT is involved in regulating the balance between apoptosis and proliferation in lung carcinomas. *Anticancer Res* 2007; 27: 575-581.

E18. Pugh ME, Hemnes AR. Pulmonary hypertension in women. *Expert Rev Cardiovasc Ther* 2010; 8: 1549-1558.

E19. Rabelo RA, Antunes LM, Etchebehere RM, Nomelini RS, Nascentes GA, Murta EF, Pedrosa AL. Loss of heterozygosity in the fragile histidine triad (FHIT) locus and expression analysis of FHIT protein in patients with breast disorders. *Clin Exp Obstet Gynecol* 2013; 40: 89-94.

Table E1

Patient demographics

A Transformed lymphocytes

Patient ID		Sex	Age at time of study	Age at discovery	Survival since discovery	% disease free years	BMPR2 NMD Status	Relation
Family1	P1a	M	53	43	10	81	NMD+	
	P1b	F	39	25	14	64	NMD+	2nd cousin of P1a
	C1	F	74			100	NMD+	distant cousin of P1a and P1b
	C1b	M	81			100	NMD+	Father of P1a
Family2	P2	F	43	35	8	81	unlikely, not confirmed	
	C2	F	72			100	unlikely, not confirmed	mother of P2
Family3	P3	F	39	28	11	72	NMD-	
	C3a	M	39			100	NMD-	Distant cousin of P3
	C3b	F	50			100	NMD-	aunt of P3
Family4	P4	M	50	38	12	76	NMD+	
	C4	F	56			100	NMD+	distant cousin of P4
Family5	P5	M	49	34	15	69	unlikely, not confirmed	
	C5	M	63			100	unlikely, not confirmed	uncle of P5
Family6	P6a	F	65	28	37	43	NMD+	niece of P6b
	P6b	F	82	64	18	78	NMD+	
	C6	M	85			100	NMD+	brother of 6b, uncle of P6a
Family7	P7	F	48	37	11	77	NMD+	
	C7	M	71			100	NMD+	uncle of P7
unrelated	P8	F	34	29	5	34	NMD-	
	C8	F	67			100	NMD-	
Controls		F n=7 M n=3						

B PAECs

Group	Diagnosis	Sex	Age at time of study	Racial background	
Controls		F n=3 M n=3	38.7 ± 8.1554	Caucasian n=5 Unknown n=1	
Patients	IPAH n=7 FPAH n=2 N/K n=1	F n=7 M n=3	35.1 ± 2.8889	Caucasian n=8 African American n=1 Hispanic n=1	

C Lung histology

Patient ID	Diagnosis	Sex	Age	Racial Background
CC-015	FPAH	F	33	Caucasian

Table E1: Summary of patient demographics including age, sex, PAH group, mutational status when available the patient samples used (transformed lymphocytes, pulmonary artery endothelial cells and lung histology).
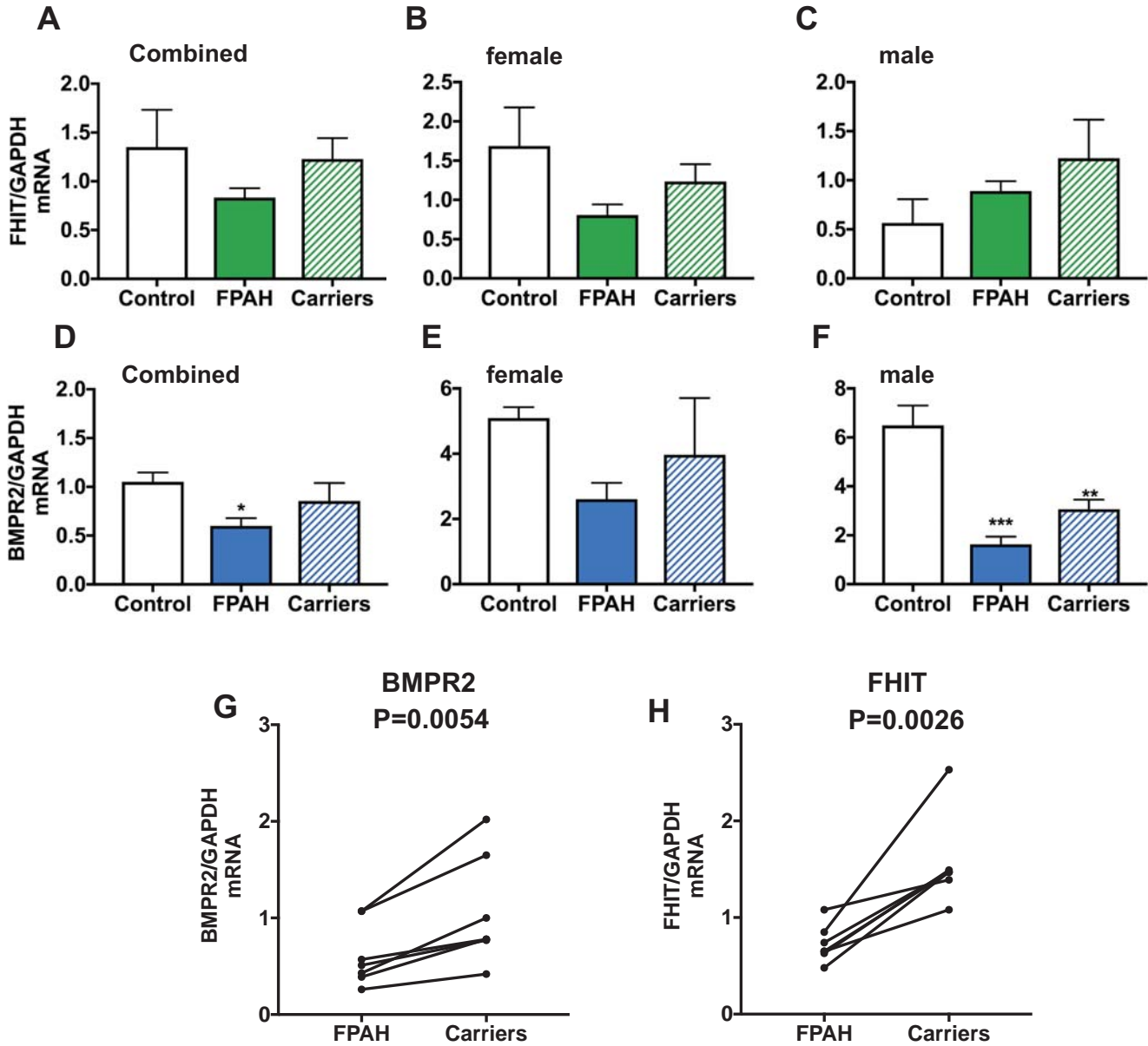
Figure E1: Sex difference in BMPR2 expression in FPAH and Carriers versus healthy controls

qPCR mRNA analysis of FHIT (A-C) and BMPR2 (D-F) expression in transformed lymphocytes from selected families with FPAH patients and healthy mutation carrier compared to healthy controls analyzed for females (B,E), males (C,F) and combined subjects (A,D). N=10, Mean ± SEM, * p < 0.05, One-Way ANOVA, Dunnett's post-test, for patient demographics see Table E1. (G,H) Graphic display of BMPR2 and FHIT expression in FPAH patients compared to the carriers of the same family. Paired t-test p=0.0054 BMPR2, p=0.0026 FHIT.

Figure E2
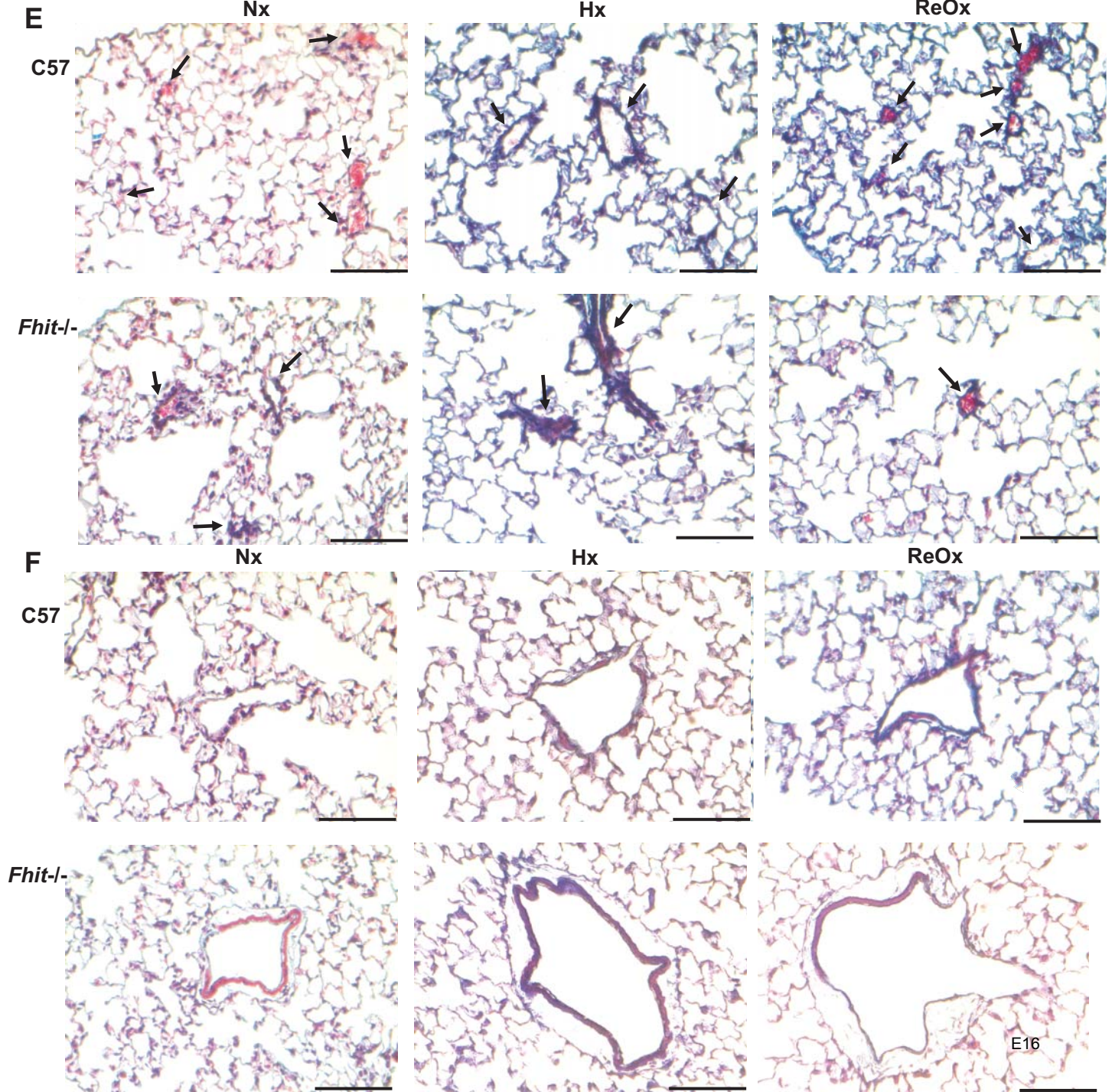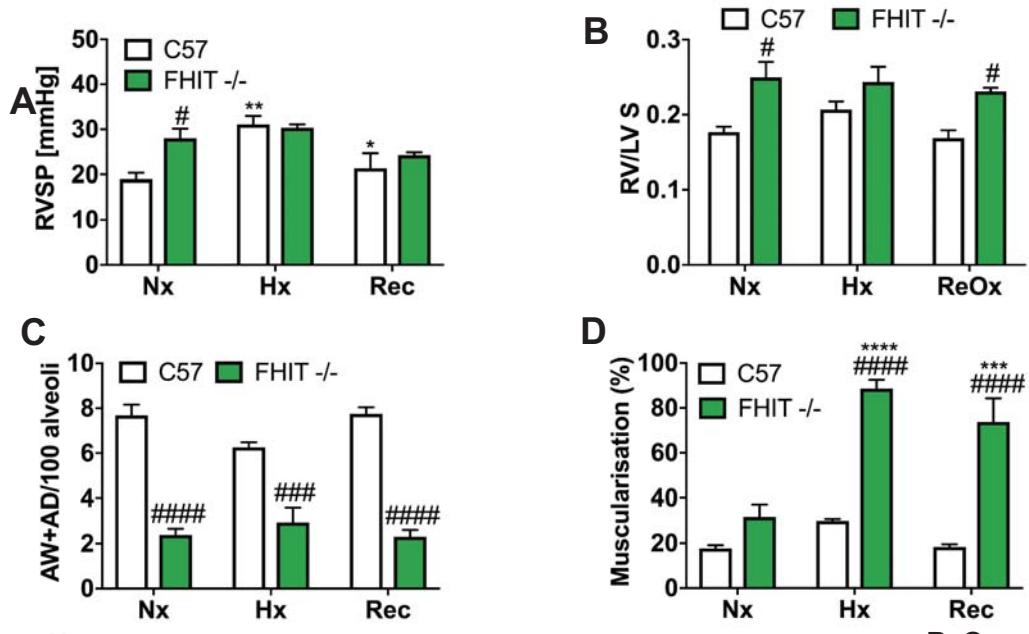
Figure E2: *Fhit-/-* C57BL/6 mice develop experimental PAH after chronic exposure to Hypoxia. Female *Fhit-/-* C57BL/6 vs. littermate wildtype (C57) mice were housed for three weeks in normoxic (Nx, 20% O2), hypoxic (Hx, 10 % O2) conditions, a hypoxia-recovery (Rec, 3 weeks Hx/4 weeks Nx) period for 4 weeks, compared to 7 weeks Nx controls. **A**, Right ventricle systolic pressure (RVSP) was measured by pulmonary artery catheterisation (female, C57 n=3, FHIT -/- Nx n=4, FHIT -/- Hx Rec n=3). **B**, Right ventricle (RV) hypertrophy is demonstrated by the weight ratio of RV to left ventricle and septum (RV/LV+S) (female, C57 n=3, *Fhit-/-* Nx n=4, FHIT -/- Hx n=3, *Fhit-/-* Rec n=5). **C**, Loss of alveolar wall (AW) and alveolar duct (AD) pulmonary vessels. **D**, Full or partial muscularization (%) of AW or AD vessels was assessed in MOVAT stained lung sections (female, C57 n=3, *Fhit-/-* Nx n=4, *Fhit-/-* Hx Rec n=3). **E-F**, Representative MOVAT lung histology representing vessel loss of small distal vessels (**E**) or vessel muscularisation (**F**). Arrows indicate vessel position. Scale bars represent 200 µm. All bars denote Mean ± SEM. * $p < 0.05$, ** $p < 0.01$, *** $p < 0.001$, **** $p < 0.0001$ vs. Nx control, # $p < 0.05$, ### $p < 0.001$, #### $p < 0.0001$ vs. C57 control, Two Way ANOVA, Turkey's post-test.

Figure E3
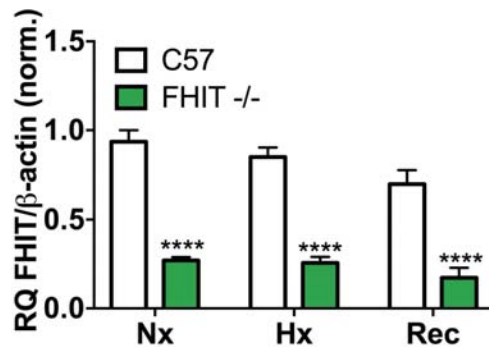
Figure E3: FHIT protein expression in *Fhit-/-* mice compared to C57BL/6 controls in normoxia versus 3 weeks chronic hypoxia as well as 4 weeks re-oxygenation.
Fhit-/- C57BL/6 vs. littermate wildtype (C57) mice were housed for three weeks in normoxic (Nx, 20% O2), hypoxic (Hx, 10 % O2) conditions, a hypoxia-recovery (Rec, 3 weeks Hx/4 weeks Nx) period for 4 weeks, compared to 7 weeks Nx controls. Representative densitometric analysis of FHIT protein expression in lung tissue normalised to a β-actin housekeeping control (male, C57 n=3, *Fhit-/-* Nx n=3, *Fhit-/-* Hx n=5, *Fhit-/-* Rec n=4). All bars denote Mean ± SEM. **** $p < 0.0001$ vs. C57 control, Two Way ANOVA, Turkey's post-test.
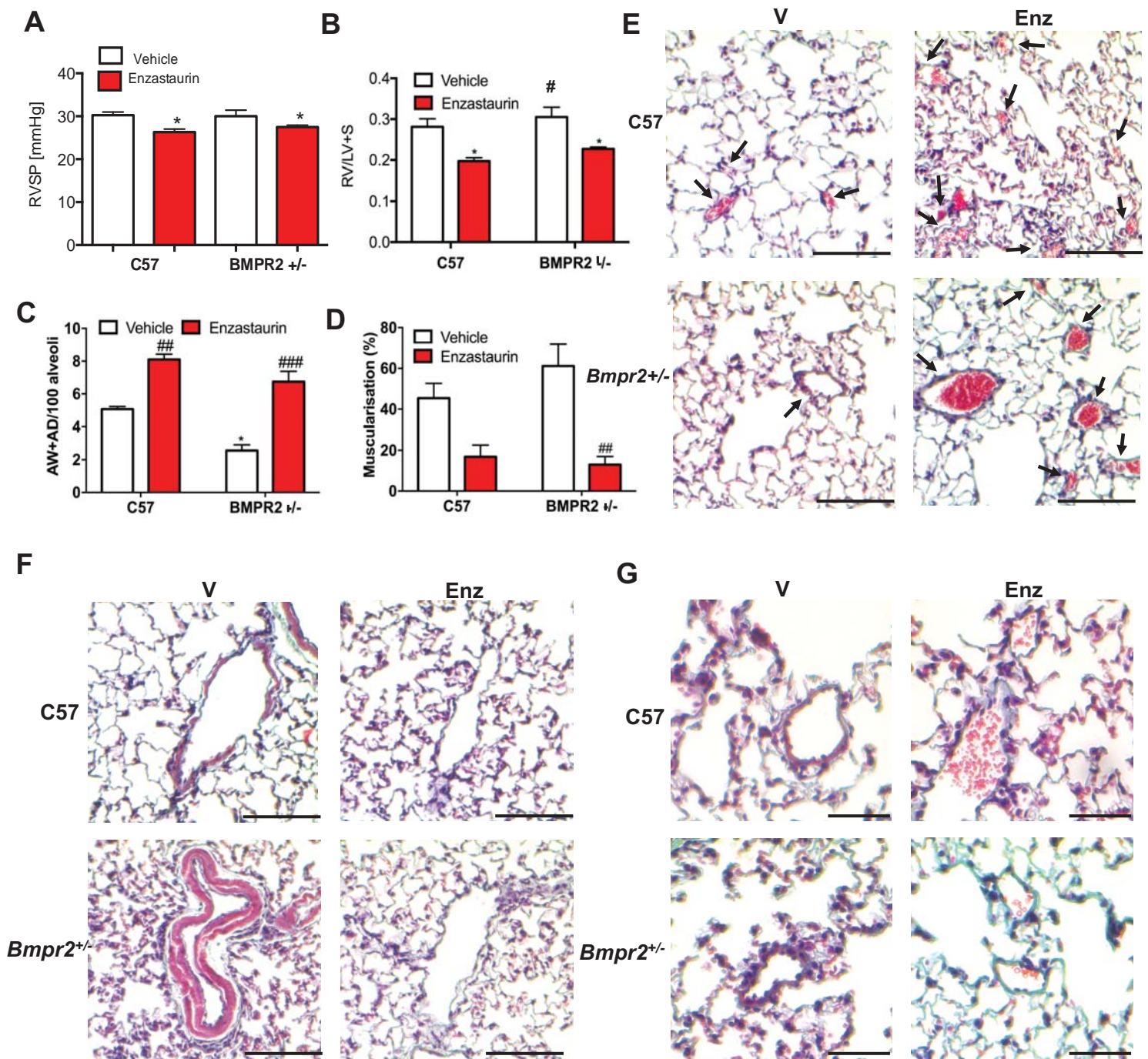
Figure E4

Figure E4: Enzastaurin prevents the development of hypoxia-induced experimental PAH in C57BL/6 and BMPR2 +/- mice. Male Wildtype and *Bmpr2+/-* C57BL/6 (C57) mice were housed for three weeks in normoxic (Nx, 20% O2) and hypoxic (Hx, 10 % O2) conditions, treated with or without daily administration of 5 mg/kg Enzastaurin by oral gavage/ Alzet mini-osmotic pump model 2006. A, Right ventricle systolic pressure (RVSP) was measured by pulmonary artery catheterisation (n=3, Mean ± SEM, * p < 0.05 vs. Nx control, One Way ANOVA, Sidak's post-test). B, Right ventricle (RV) hypertrophy is demonstrated by the weight ratio of RV to left ventricle and septum (n=3, Mean ± SEM, # p < 0.05 vs. vehicle control, Two Way ANOVA, Turkey's post-test). C, Loss of alveolar wall (AW) and alveolar duct (AD) pulmonary vessels and D, their full or partial muscularization (%) was assessed in MOVAT stained lung sections (n=3, Mean ± SEM, * p < 0.05 vs. C57 control, ## p < 0.01, ### p< 0.001 vs. vehicle control, Two Way ANOVA, Turkey's post-test). E, Representative MOVAT lung histology. Arrows indicate vessel position. Scale bars represent 200 μm. F-G, Representative MOVAT lung histology of large (F) and small vessels (G) respectively. Arrows indicate vessel position. Scale bars represent 200 or 50 μm, as indicated.
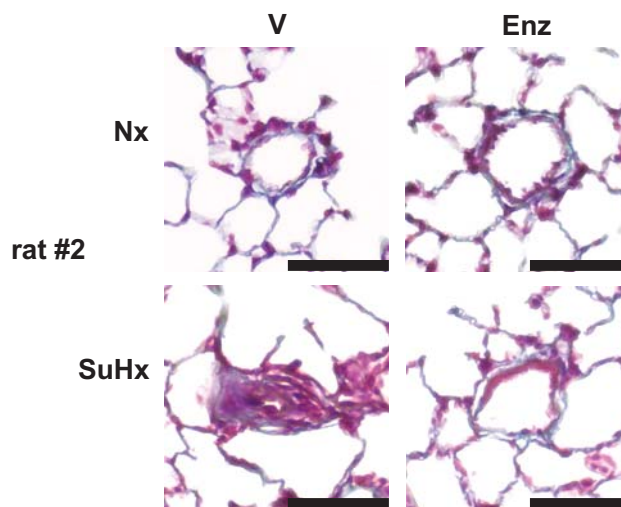
Figure E5

Figure E5: Representative MOVAT lung histology in Sprague Dawley rat lungs, comparing Normoxia and Sugen/Hypoxia conditions after 3 weeks of Enzastaurin treatment.
Experimental PAH was induced in male Sasco Sprague Dawley rats by subcutaneous injection of 20 mg/kg body weight SU5416. Animals were housed for 3 weeks in hypoxic (Hx, 10 % O2) conditions, followed by a 5 week period in normoxia (Nx, 20% O2), following daily administration of 5 mg/kg body weight Enzastaurin or vehicle control by oral gavage.
Representative MOVAT lung histology of small pulmonary vessels are shown. Scale bars represent 20 μM.
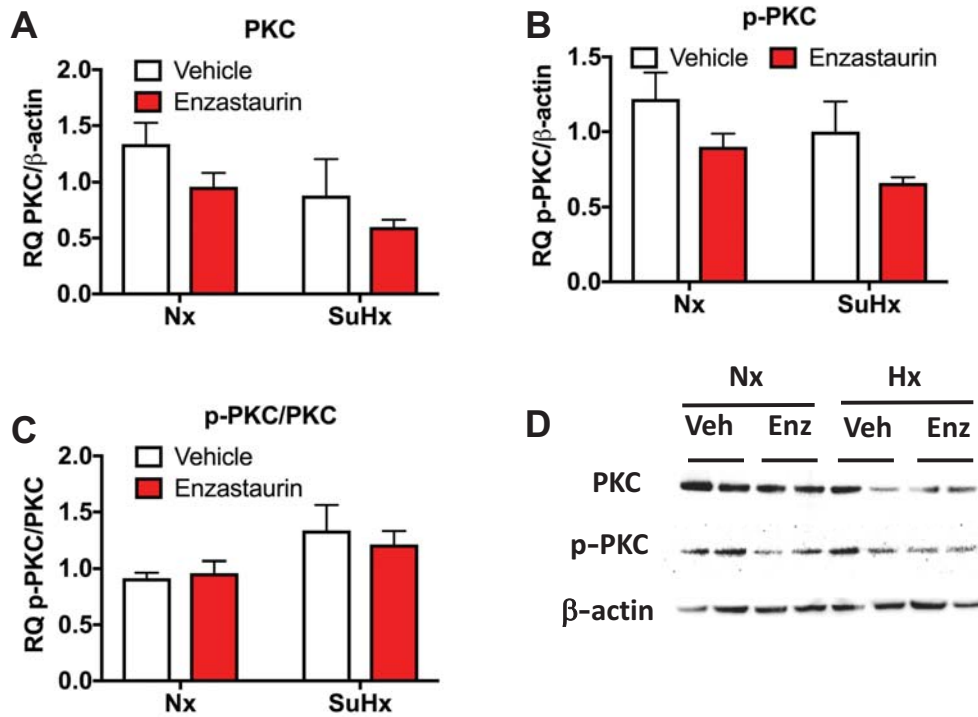
Figure E6

Figure E6: PKC and p-PKC protein expression in Sprague Dawley rat lungs, comparing Normoxia and Sugen/Hypoxia conditions after 3 weeks of Enzastaurin treatment.
Experimental PAH was induced in male Sasco Sprague Dawley rats by subcutaneous injection of 20 mg/kg body weight SU5416. Animals were housed for 3 weeks in hypoxic (Hx, 10% O2) conditions, followed by a 5 week period in normoxia (Nx, 20% O2), following daily administration of 5 mg/kg body weight Enzastaurin or vehicle control by oral gavage.
Densitometric analysis of PKC (**A**) and p-PKC (**B**) protein expression in lung tissue normalised to a β-actin housekeeping control (male, Nx n=4, Nx Enz n=4, SuHx n=3, SuHx Enz n=5) and p-PKC normalised to PKC (**C**). Representative blots of PKC, p-PKC and β-actin (**D**). All bars denote Mean ± SEM. Two Way ANOVA, Turkey's post-test.

Figure E7

C57Bl6 – WT mice - Hypoxia
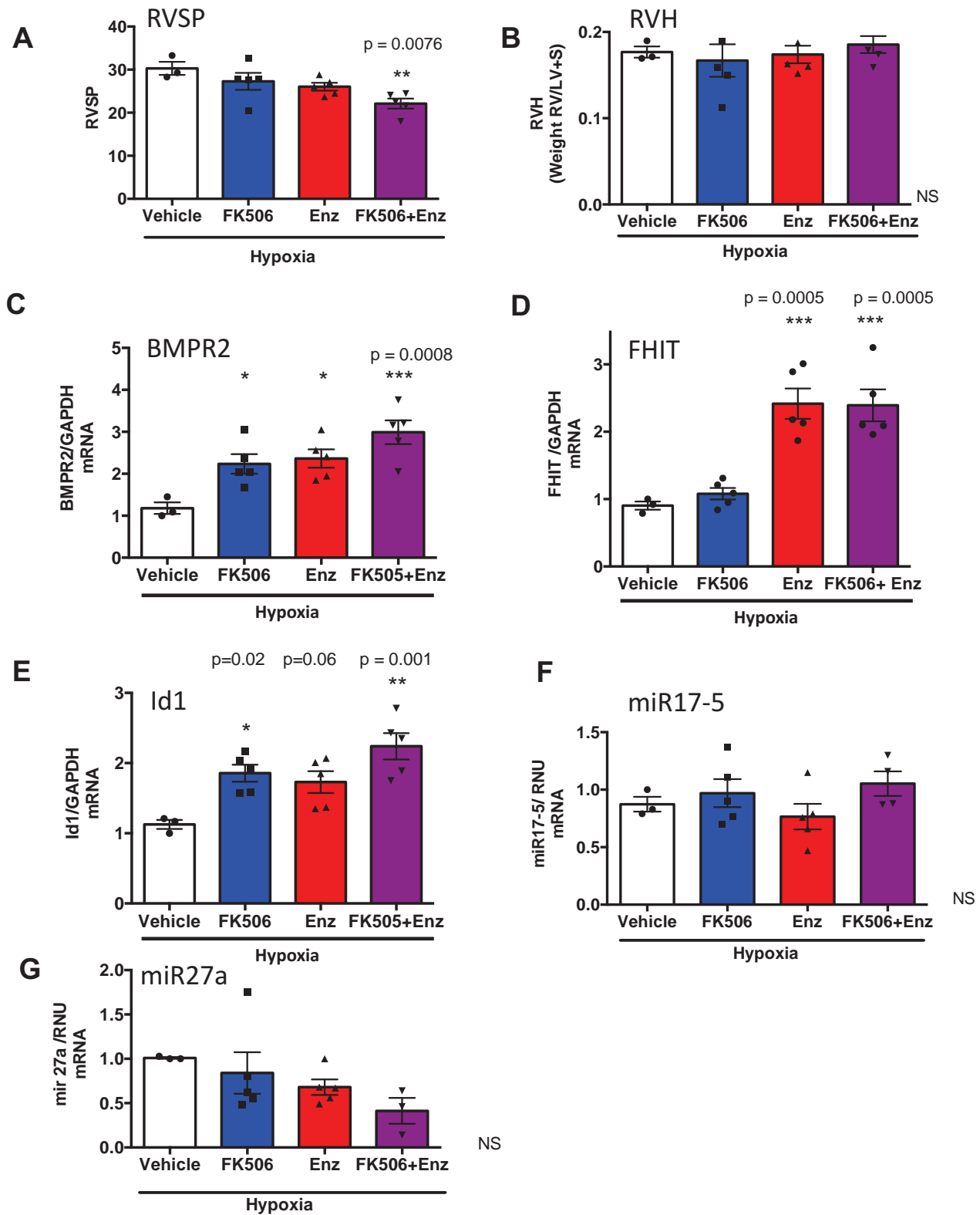
Figure E7: FK506 and Enzastaurin combined prevent hypoxia induced pulmonary hypertension and show an additive effect on BMPR2 and Id1 (not FHIT) mRNA expression. Male Wildtype C57BL/6 (C57) mice were exposed to three weeks in hypoxic (Hx, 10 % O2), and treated with 5mg/kg body weight Enzastaurin or vehicle control (saline) with or without 0.05mg/kg/d FK506 by mini-osmotic pump (Alzet model 2004). **A** Right ventricle systolic pressure (RVSP) was measured by pulmonary artery catheterisation (n=3, Mean ± SEM, ** p < 0.01 vs. Sham control, One Way ANOVA, Dunnett's post-test). **B** Right Ventricular Hypertrophy as measured by weight RV/LV+S. **C-F**, ΔΔCt analysis of mRNA expression in lung tissue. (n=3, Mean ± SEM, * p < 0.05, ** p < 0.01, *** p < 0.001 vs. Vehicle control, One Way ANOVA, Dunnett's post-test). Abbreviations: Enz – Enzastaurin.
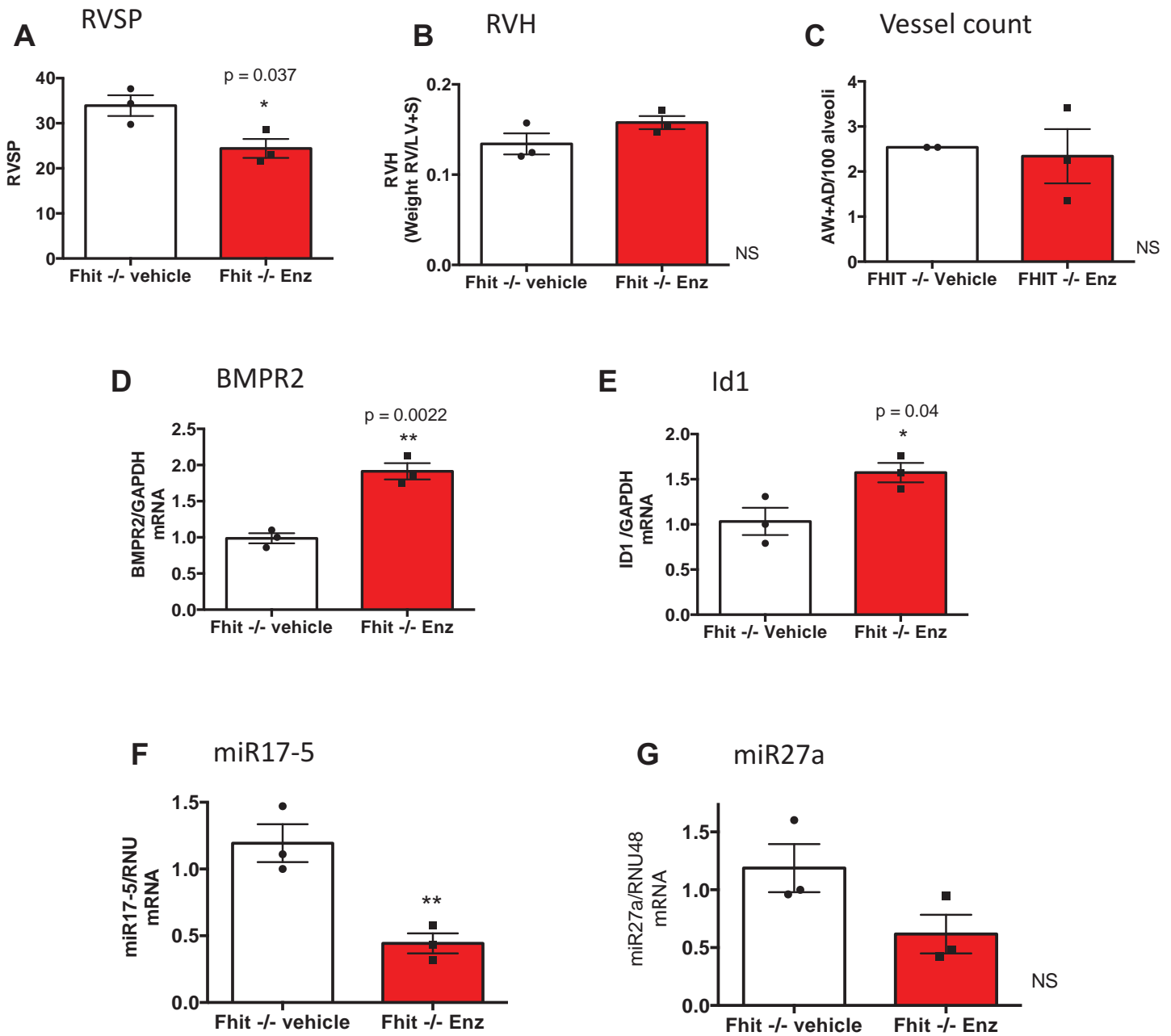
Figure E8: Enzastaurin prevents pulmonary hypertension in FHIT -/- mice exposed ti hypoxia through miR17-5 mediated upregulation of BMPR2 and Id1
Male *FHIT-/-* mice were exposed to three weeks hypoxia (Hx, 10 % O2), treated with Enzastaurin or vehicle (saline) control at a concentration of 5mg/kg body weight by mini-osmotic pump (Alzet model 2004). **A**, Right ventricle systolic pressure (RVSP) was measured by pulmonary artery catheterisation (n=3, Mean ± SEM, * p < 0.05 vs. vehicle control, unpaired Student's t test). **B** Right Ventricular Hypertrophy (RVH) as measured by weight of the RV/ LV+ Septum. **C** Number of alveolar wall and alveolar duct vessel/ 100 alveoli (4-5 20 x fields per mouse). **D--G**, ΔΔCt analysis of mRNA expression in lung tissue. (n=3, Mean ± SEM, * p < 0.05, ** p < 0.01 vs. Vehicle control, unpaired Student's t test). Abbreviations: Enz – Enzastaurin
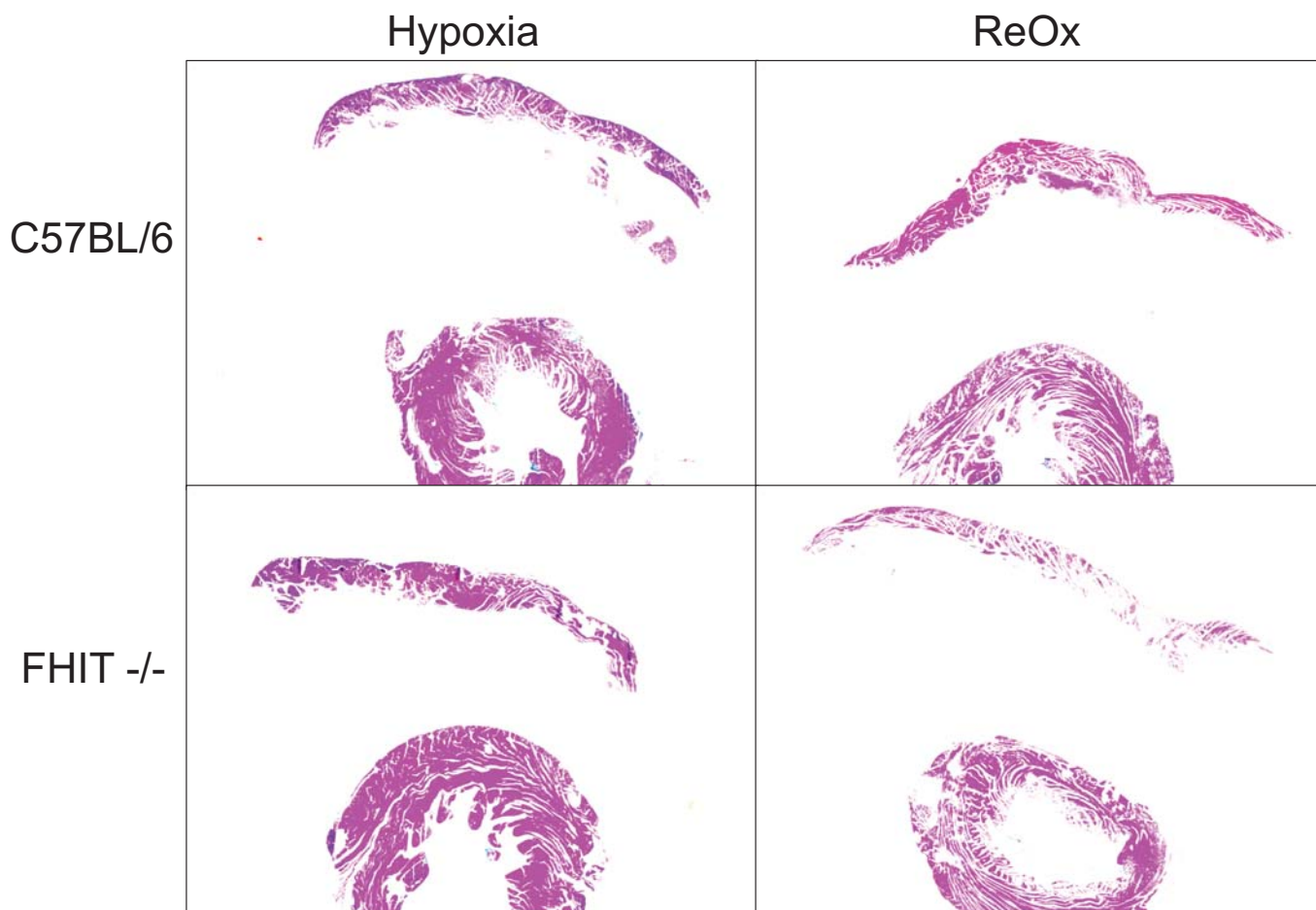
Figure E9

	Hypoxia	ReOx

C57BL/6

FHIT -/-

Figure E9: WT and *FHIT -/-* C57BL/6 mice do not develop RV fibrosis following hypoxic treatment.
Male Wildtype and *FHIT-/-* C57BL/6 (C57) mice were housed for three weeks in hypoxic (Hx, 10 % O2) conditions and a hypoxia-recovery (Rec, 3 weeks Hx/4 weeks Nx) period for 4 weeks. Representative Trichrome heart histology is shown. Fibrosis is indicated by the blue colour.
The RV and LV+Septum had to be separated from each other for weight RV/LV+Septum assessment.

Figure E10
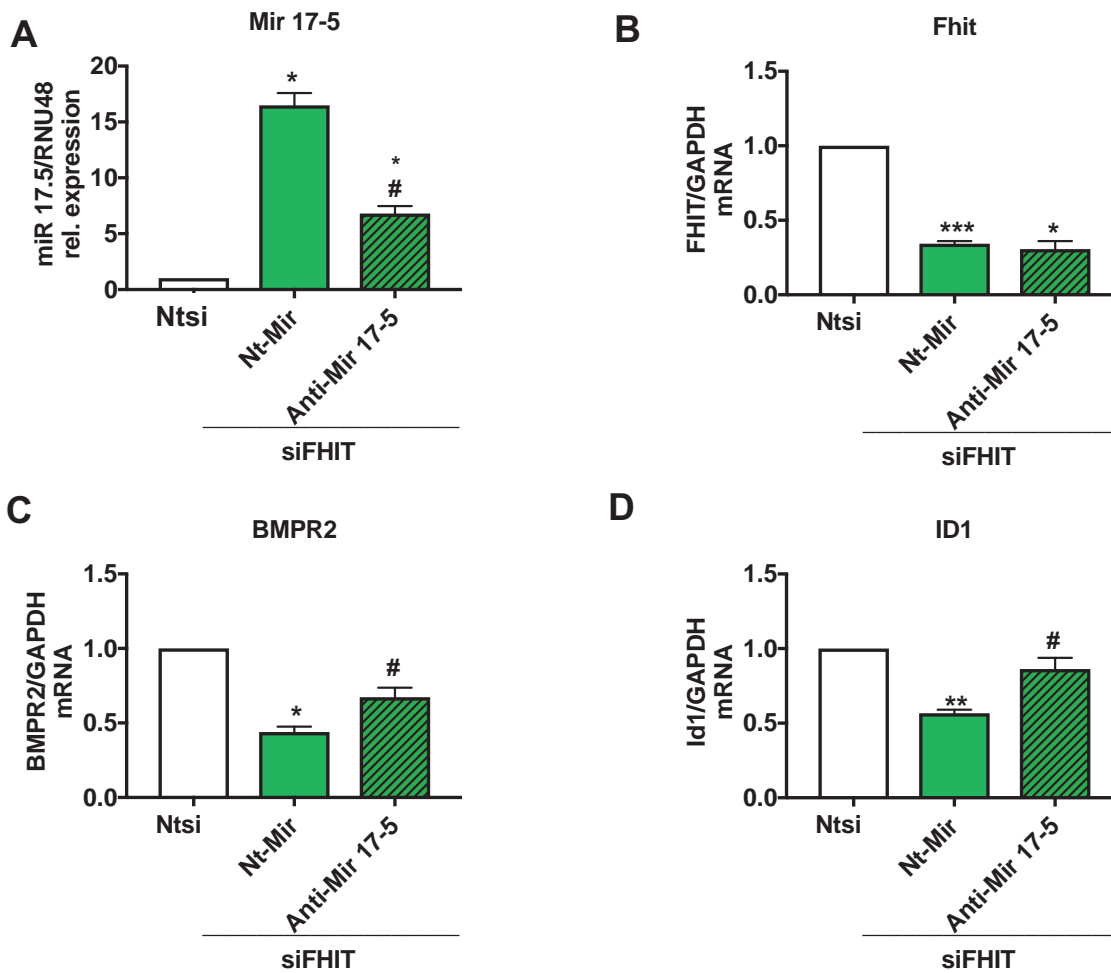
Figure E10: Reduction of BMPR2 and ID1 in PAEC by FHIT knockdown is in part miR17-5 dependent. Human PAEC were plated on the 6 well plates (0.5×10^6 cells/well) and transfected with siFhit (Ambion Silencer ®select, P/N 4392420) 100nM and anti-miR 17-5 inhibitor (AM12412, Ambion) by RNAiMax for 48 hours. Anti-miR MiRNA inhibitor was used as the negative control (AM17010, Ambion)l. MiRNA was isolated by TaqMan® miRNA ABC purification kit and the isolated miRNA was analyzed using Taqman® MicroRNA assays. Fhit, BMPR2 and Id1 gene expression was measured using Taqman® gene expression assay and normalized to GAPDH whereas miR17-5 was normalized to RNU48 (**A**) Relative expression of miR17.5 (**B**) FHIT, (**C**) BMPR2 and (**D**) ID1. All bars denote Mean ± SEM., n=3, * $p < 0.05$, ** $p < 0.01$, *** $p < 0.001$ vs. Ntsi, One Way ANOVA, Turkey's post-test, # $p < 0.05$ vs. NtMir, unpaired Student's t test,
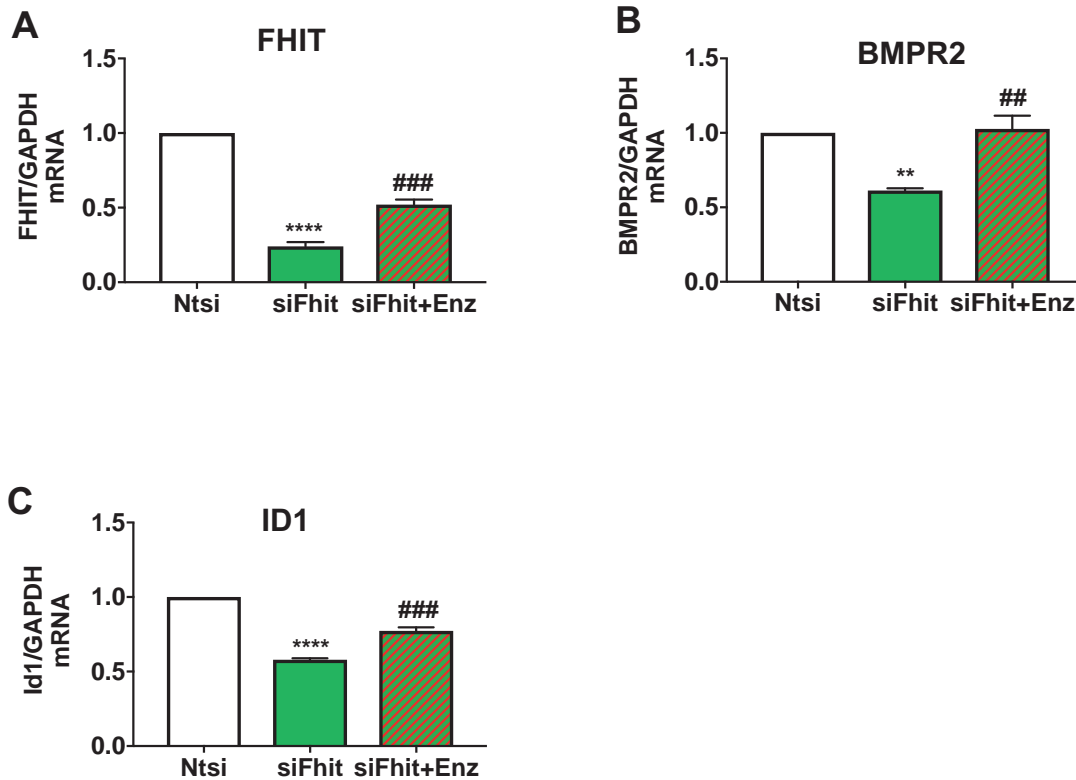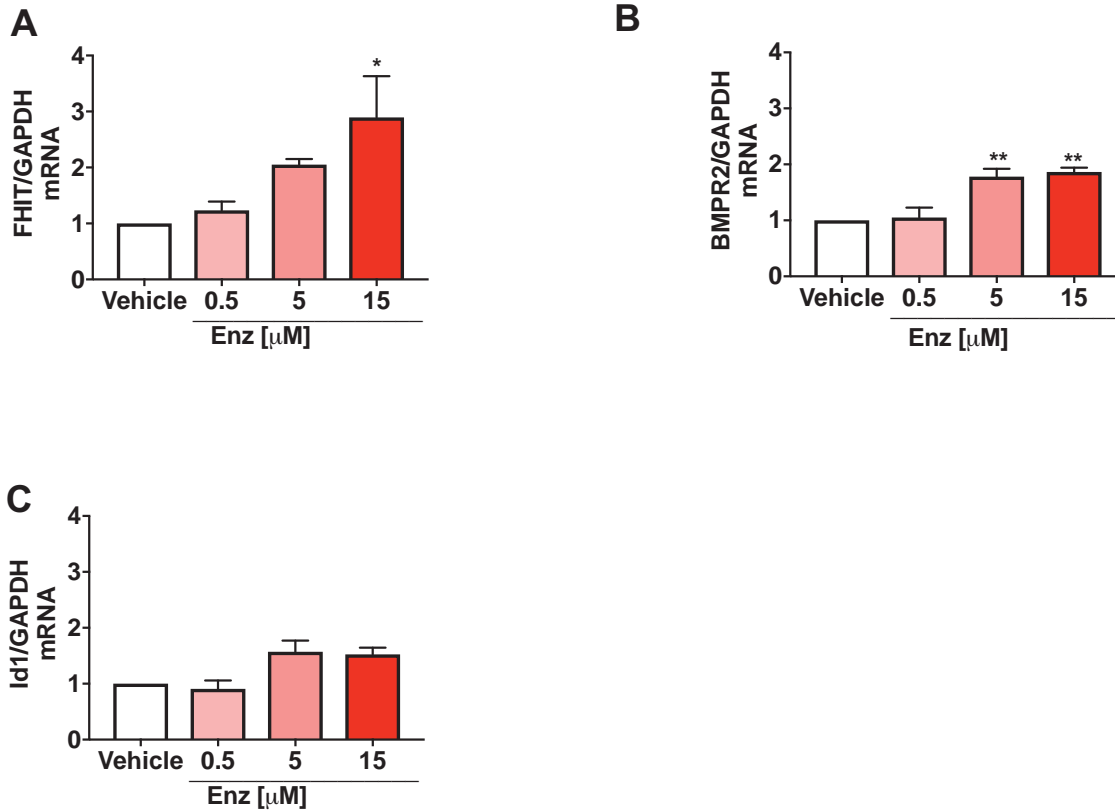
Figure E11

Figure E11: 24 h treatment with Enzastaurin increases FHIT, BMPR2 and Id1 expression in PAECs in which FHIT is reduced by siRNA. Human PAEC were plated on the 6 well plates (0.5x10^6 cells/well) and transfected with siFhit (Ambion Silencer ®select, P/N 4392420) 100nM and then treated with Non-targeting siRNA 100nM by RNAiMax (Invitrogen) for 48 hours. Cells were then treated with Enzastaurin 15 uM for 24 hours. RNA was isolated by RNeasy® Plus Mini Kit (Qiagen) and analyze Fhit, BMPR2 and Id1 gene expression by Taqman® gene expression assay (Invitrogen. Fhit, BMPR2 and Id1 gene expression was measured using Taqman® gene expression assay (**A**) Relative expression of FHIT (**B**) BMPR2, (**C**) ID1. All bars denote Mean ± SEM., n=3, One Way ANOVA, Sidack's multi comparison test **** $p < 0.0001$, ** $p<0.01$ Ntsi vs siFHIT , ### $p<0.0005$, ## $P<0.01$ siFHIT vs siFHIT+Enz.

Figure E12

Figure E12: 24 h treatment with Enzastaurin increases FHIT, BMPR2 and Id1 expression in PAECs in which FHIT is reduced by siRNA. Human PAEC were plated on 6 well plates. When being 70-80% confluent, cells were treated with Enzastaurin at $0.5\mu M$, $5\mu M$ and $15\mu M$ respectively for 24 hours. RNA was isolated by RNeasy® Plus Mini Kit (Qiagen) and Fhit, BMPR2 and Id1 gene expression was measured by Taqman® gene expression assay. (**A**) Relative expression of FHIT (**B**) BMPR2, (**C**) ID1. All bars denote Mean ± SEM., n=3, One Way ANOVA, Dunnet's comparison test * $p<0.05$, ** $p<0.01$ compared to control.
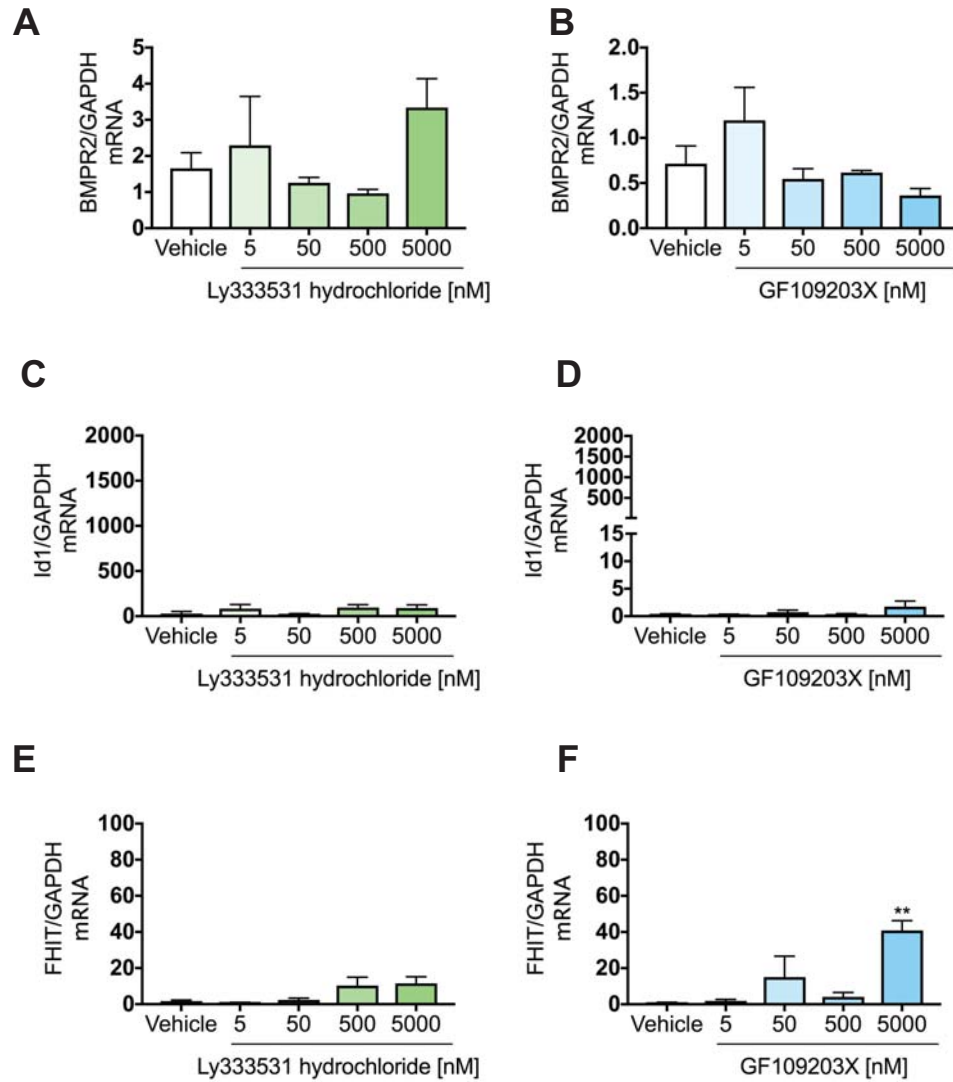
Figure E13

Figure E13: PKC inhibition by pharmaceutical PKC inhibitors, other than Enzastaurin, does not increase BMPR2-signaling and FHIT expression.
A-B, Relative mRNA expression of BMPR2 normalised to GAPDH in synchronised PAECs incubated for 24 hours with varying concentrations (5nM – 5μM) of (**A**) the selective PKCβ inhibitor Ly333531 hydrochloride (**B**) or the non-selective PKC-inhibitor GF109203X (qPCR, t= 24h, n=3, Mean ± SEM, One Way ANOVA, Dunnett's post-test, NS). **C-D**, Relative mRNA expression of Id1 normalised to GAPDH in synchronised PAECs incubated for 24 hours with varying concentrations (5nM – 5μM) of (**C**), the selective PKCβ inhibitor Ly333531 hydrochloride (**D**) or the non-selective PKC-inhibitor GF109203X (**F**) (qPCR, t= 24h, n=3, Mean ± SEM, One Way ANOVA, Dunnett's post-test, NS). **E-F**, Relative mRNA expression of FHIT normalised to GAPDH in synchronised PAECs incubated for 24 hours with varying concentrations (5nM – 5μM) of (**E**), the selective PKCβ inhibitor Ly333531 hydrochloride (**F**) or the non-selective PKC-inhibitor GF109203X (**I**) (qPCR, t= 24h, n=3, Mean ± SEM, ** $p < 0.01$, vs. vehicle control, One Way ANOVA, Dunnett's post-test).

Figure E14

Inhibitors:
Enzastaurin: PKCβ selective inhibitor
LY333531 hydrochloride – PKCβ selective inhibitor
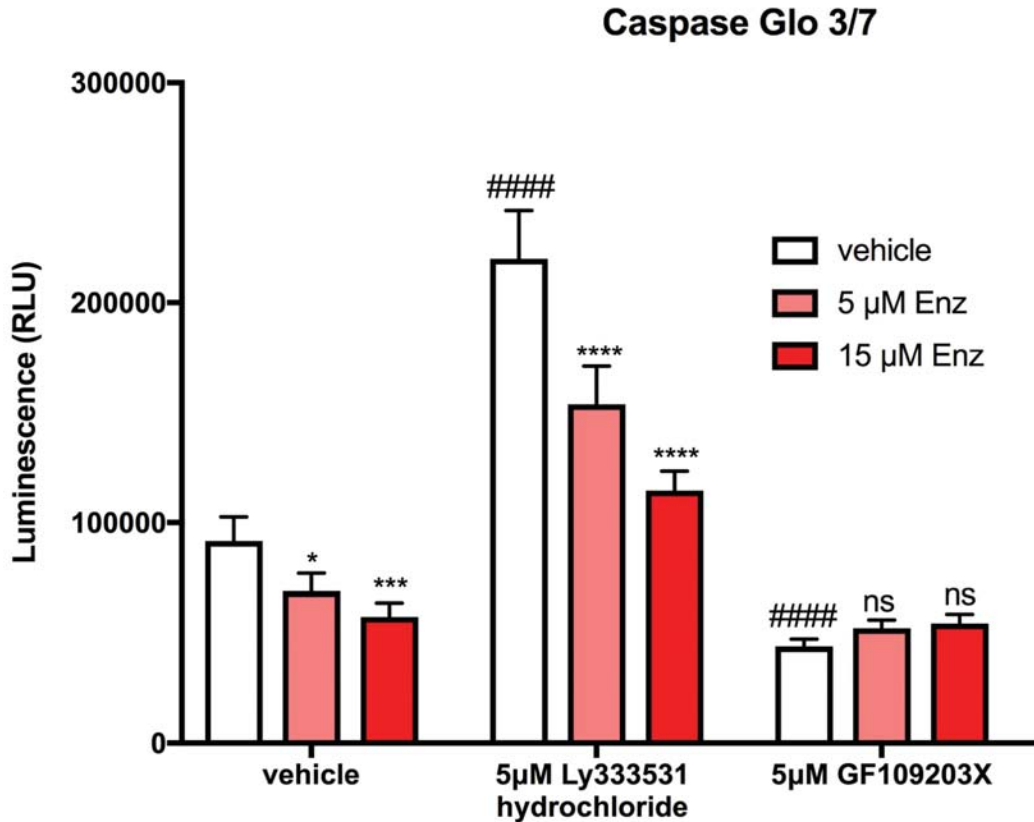GF109203X ATP – competitive broad-spectrum PKC inhibitor

Figure E14: Enzastaurin, but not PKCβ inhibitor Ly333531, decreases Caspase 3/7-mediated apoptosis in PAECs.
Caspase 3/7 luminescence in synchronised PAECs incubated for 24 hours with 5μM or 15μM of Enzastaurin (red bars) and/or 5μM of the selective PKCβ inhibitor Ly333531 hydrochloride or 5μM of the non-selective PKC-inhibitor GF109203X (t= 24 h, Caspase-Glo® 3/7 Assay, n=3, Mean ± SEM, * p < 0.05, *** p < 0.001, **** p < 0.0001 vs. non-Enzastaurin treated control, #### p < 0.0001 vs. untreated vehicle control, Two-Way ANOVA, Dunnett's post-test).
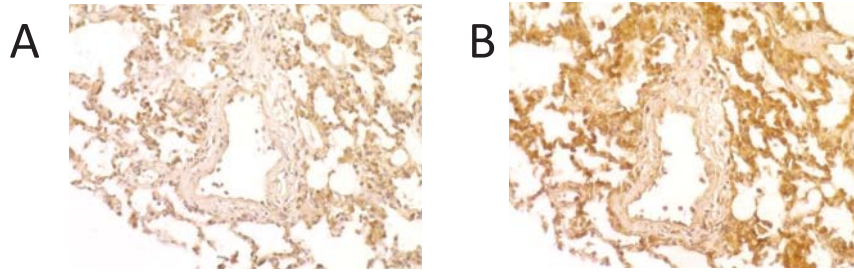
Figure E15

Figure E15: Representative Immunohistochemistry slides from IPAH patient (without a BMPR2 mutation)
A: BMPR2 expression **B**: FHIT expression.
FHIT reduction is mainly localized in neointima.
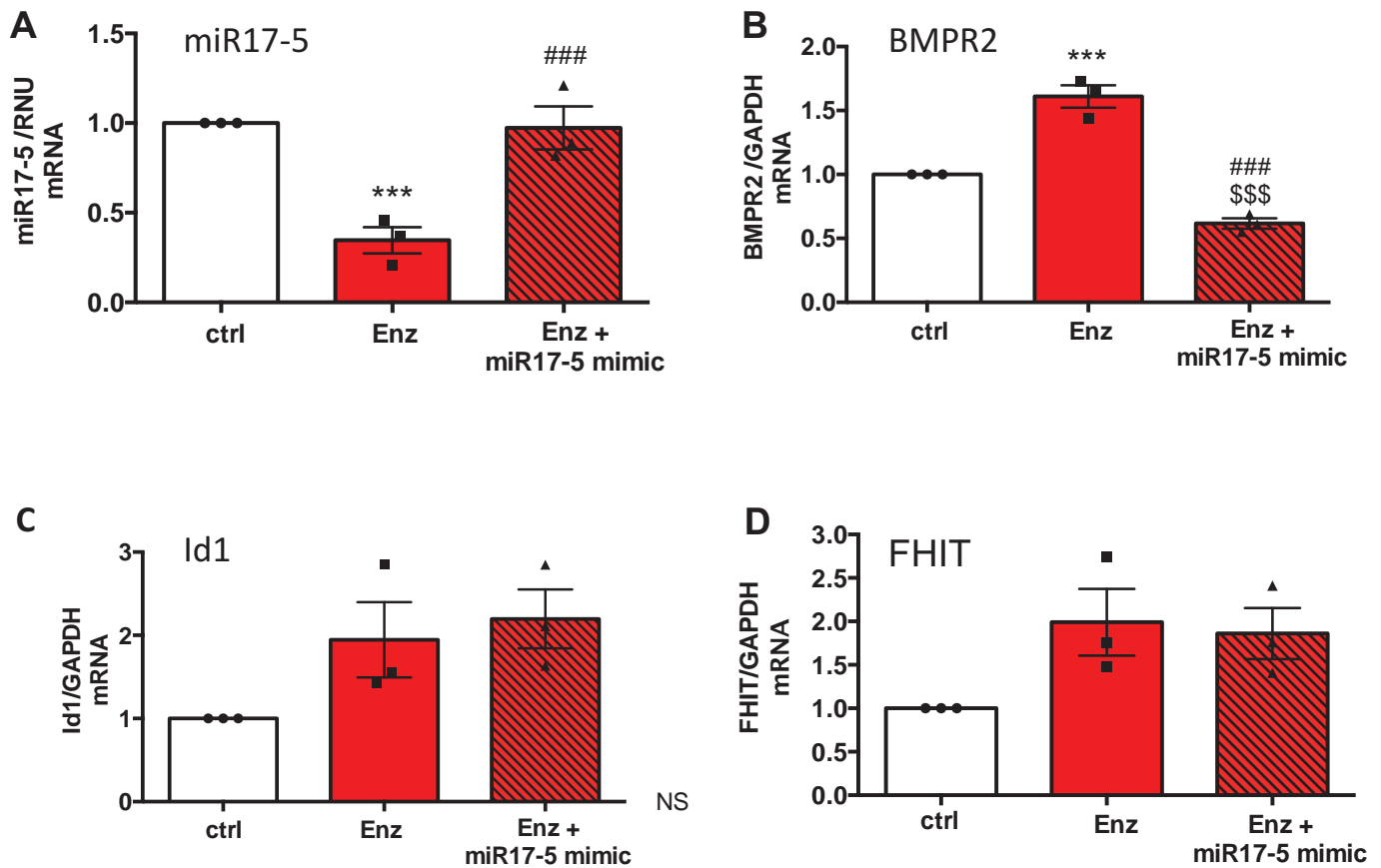
Figure E16

PAECs

Figure E16: Enzastaurin increases BMPR2 expression via downregulation of miR17-5, whereas Enzastaurin mediated Id1 signaling is not solely dependent on miR17-5 downregulation

Human PAEC were plated on the 6 well plates (0.5×10^6 cells/well) and transfected withmiR17-5 mimic (AM12412, Ambion) 100nM by RNAmx for 48 hours and treated with Enzastaurin 15 uM for 24 hours. RNA was isolated by RNeasy® Plus Mini Kit (Qiagen) and BMPR2, Id1 and FHIT gene expression was analyzed by Taqman® gene expression assay. MiRNA was isolated by TaqMan® miRNA ABC purification kit and miR17-5 was analyzed using Taqman® MicroRNA assays (**A**) Relative expression of mIR17-5 normalized to RNU48 (**B**) BMPR2, (**C**) ID1 and (**D**) FHIT All bars denote Mean ± SEM., n=3, One Way ANOVA, Sidack's multi comparison test *** $p < 0.001$, ** $p < 0.01$ Enz vs ctrl , ### $p < 0.005$ Enz + miR vs Enz, $$$ $p < 0.005$ Enz+miR vs ctrl.
Enz: Enzastaurin.